Volume 1
Number 2
April 2025
Pages 211-330

EES Batteries

rsc.li/EESBatteries

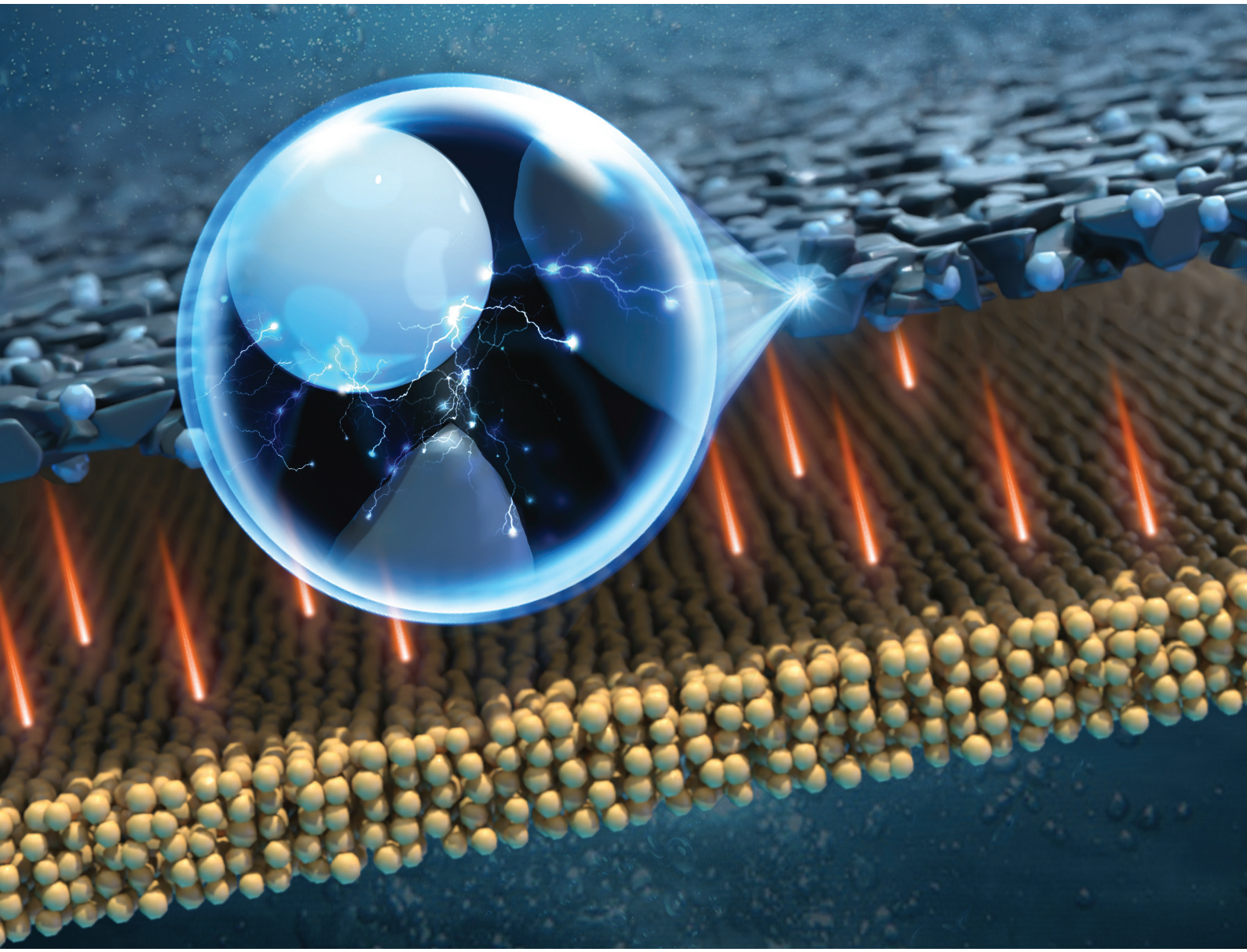

ISSN 3033-4071

ROYAL SOCIETY OF CHEMISTRY

PAPER
Lili Gong, Peng Tan *et al.*
Li^+ crosstalk-driven calendar aging in Si/C composite anodes

EES Batteries

ROYAL SOCIETY OF CHEMISTRY

PAPER

View Article Online
View Journal | View Issue

Cite this: *EES Batteries*, 2025, **1**, 250

Li^+ crosstalk-driven calendar aging in Si/C composite anodes†

Kai Sun,[a] Xueyan Li,[a] Kang Fu,[a] Zhuojun Zhang,[a] Anmin Wang,[a,b] Xingmin He,[a] Lili Gong*[a] and Peng Tan *[a,c]

Received 3rd December 2024,
Accepted 6th January 2025

DOI: 10.1039/d4eb00040d

rsc.li/EESBatteries

To meet the demand for high-energy density, lithium-ion batteries (LIBs) with silicon/graphite (Si/C) composite anodes are capturing an increasing share of the market. Contrary to the common belief of low self-discharge, we demonstrate that LIBs with anodes containing 15 wt% Si retain only 77.7% of their capacity after 24 h of storage at room temperature. We quantitatively analyse the impact of Si addition on calendar aging, emphasizing the critical role of Li^+ crosstalk during storage through a synergy of cross-scale characterizations and multidimensional simulations. Si induces severe side reactions, leading to significant Li loss and potential jump. To balance inter-particle potentials, graphite is compelled to transfer Li^+ to Si, resulting in additional capacity loss. Theoretical calculations indicate that modifying the Li^+ crosstalk pathway can suppress self-discharge, for instance, by increasing the Li diffusion coefficient (D_{Li^+}) of active materials. To validate this approach, the Si@C material with a higher D_{Li^+} is synthesized, and the improved batteries with anodes containing 15 wt% Si@C retain 93.0% of their capacity after 24 h of storage. This work uncovers the underlying impact of Li^+ crosstalk on calendar aging, offering new perspectives and guidance for investigating degradation mechanisms in other composite electrode systems.

Broader context

The silicon (Si)-containing lithium-ion batteries are one of the most successful power devices. However, spontaneous side reactions between Si and electrolyte significantly shorten the calendar life of these batteries, which has long been overlooked. In this work, we integrated experimental and simulation approaches to reveal the kinetic changes in Si-containing batteries during storage. The findings highlight that Li^+ crosstalk significantly impacts calendar life: Si plunders Li^+ from graphite, compromising the stability of graphite. By enhancing the Li storage capability of Si through promoting Li diffusion coefficients, we effectively altered the self-discharge pathway, substantially suppressing the self-discharge. The calendar life demonstrated a 20% increase for cells with improved Si-containing anode after 24 h of storage. With the expanding market for Si-containing batteries, more attention must be paid to calendar aging studies, as the extra addition of active materials alters the physical and chemical environment. Besides, the combined simulation and experimental approach used here offers a reference for further studies on electrodes with composite materials.

Introduction

Lithium-ion batteries (LIBs) have served as a primary power source for electric vehicles (EVs) owing to their excellent energy density (250–300 W h kg^{-1}),[1] and long cycle life (1000 km cruise range),[2] which is helpful for sustainable and green development.[3,4] Since the graphite anode has approached its theoretical capacity (372 mA h g^{-1}),[5] to meet the demands for higher energy density,[6] cells with silicon/graphite (Si/C) composite anodes (>500 W h kg^{-1}) quickly attract attention from both academia and industry.[7–9]

Compared to traditional graphite anodes, adding Si offers advantages such as low cost (\$4.2–\$6.5 kg^{-1}), high abundance, and high specific capacity (3579 mA h g^{-1} for $Li_{3.75}Si$).[10] However, the mechanical failure caused by ~300% volume change of Si leads to rapid performance degradation.[11–13] Additionally, Si readily undergoes side reactions with the electrolyte, resulting in capacity loss.[14,15] To improve the stability of Si/C composite anodes, significant efforts have been made

[a]*Department of Thermal Science and Energy Engineering, University of Science and Technology of China (USTC), Hefei 230026, Anhui, China.*
E-mail: liligong@ustc.edu.cn, pengtan@ustc.edu.cn
[b]*Gotion High-Tech Co., Ltd, Hefei 230012, Anhui, China*
[c]*State Key Laboratory of Fire Science, University of Science and Technology of China (USTC), Hefei 230026, Anhui, China*

† Electronic supplementary information (ESI) available. See DOI: https://doi.org/10.1039/d4eb00040d

from material design to electrode preparation, such as employing nano-Si,[16] modifying material structures,[17,18] and changing binders and electrolytes.[19,20] For example, Jia *et al.* synthesized Si@C with high mechanical strength, which effectively buffers Si expansion and enables over 92% capacity retention after 500 cycles.[21] Recently, the Si-containing cells proposed by Bai *et al.* achieved an energy density of 325.9 W h kg^{-1} by combining structural optimization and gel electrolytes, maintaining 88.7% capacity retention even after 2000 cycles.[10]

Although higher energy density and cycle life have greatly inspired both academia and industry, the calendar life of these cells during storage has been habitually overlooked.[22,23] For EVs, more than 12 hours a day are spent in an idle state, which means that calendar life accounts for more than half of the total battery lifespan. Furthermore, Si-containing cells from the market were reported with calendar life far less than traditional graphite-based cells.[23] Research on calendar aging for cells with Si/C composite anodes plays a crucial role in extending lifespan and expanding market scale. During storage, Si/C composite anodes experience both active material loss (LAM) and lithium inventory loss (LLI).[24,25] No matter what aging mechanism was proposed, the main reason was considered as side reactions on Si.[26,27] The solid electrolyte interphase (SEI) on Si undergoes continuous decomposition and deposition, causing abundant Li loss.[28] However, the decay pathway among active materials (AMs) is blurry during storage.

In this work, the calendar aging pathways of cells with Si/C composite anodes were specified by combining cross-scale characterization with multidimensional simulation models. First, the accelerating effect of Si addition on calendar aging was quantified using electrochemical testing and multiple compositional analysis techniques. To reveal the kinetic process between AMs, multidimensional models were developed to capture mass transport and charge transfer within the anode supplementing with microscale characterizations. Li^+ crosstalk was identified as a key factor in calendar aging, in which the transfer of Li^+ from graphite to Si compromises the stability of graphite. Based on these findings, adjusting Li^+ crosstalk significantly suppresses calendar aging. We tried to improve the calendar life from a kinetic aspect and promote the Li storage in Si by enhancing the Li diffusion coefficient (D_{Li^+}). As a proof of concept, Si@C with a high D_{Li^+} was fabricated, and the improved Si-containing cells demonstrated an increase of 20% in calendar life after 24 h of storage. We emphasize the significant impact of Li^+ crosstalk on calendar aging, and this effect offers guidance for investigating degradation mechanisms in other composite electrode systems.

Results and discussion

The instability induced by the Si

To evaluate storage performance, cells with anodes containing varying Si contents (0 wt% to 15 wt%, marked as Gr, 5Si, 10Si, and 15Si) were charged to 4.2 V and stored at room temperature (RT) for 24 h. The open circuit potential (OCP) drops were found to be Si content dependent, ranging from a 78 mV drop for the graphite-based cell to a 123 mV drop for the cell with a 15Si anode (Fig. 1a). This self-discharge effect also leads to a noticeable difference in capacity loss (Fig. 1b). After 24 h of storage, the average state of health (SOH) was 92.4%, 89.8%, 81.4%, and 77.7% for cells with the graphite, 5Si, 10Si, and 15Si anode, respectively. Increasing Si content intensifies calendar aging. Especially for cells with 15Si anodes, internal side reactions result in complete cell failure after 24 h of storage.

The addition of Si was proven to cause severe capacity and voltage loss, and this decay is aggravated when Si content increases. A three-electrode cell with a Li reference electrode was tested to record the OCPs of the anode and cathode (Fig. S1†). The potential of the cathode hardly descended, while the potential of the anode increased obviously, leading to the decay of voltage and capacity. The anodes were disembled out after 72 h of storage and compared with the pristine lithiated state (Fig. S2†). The golden color of each pristine anode refers to a Li-rich state of graphite (LiC_6),[29,30] but the Si-containing anodes after 72 h self-discharge became black and covered with a gray film. To specify the interface changes, the interfacial components were analyzed using scanning electron microscopy with energy dispersive spectroscopy (SEM-EDS, Fig. 1c and S3†). A huge growth of Li_2CO_3 and decomposition of F-containing intermediates were discovered, which has been affirmed in our previous work.[31] The weight percentage of O shifted from pristine ~10% to more than 30% after storage, especially 40.6% for the aged 10Si anode (Fig. 1c and S3, Table S1†). Besides, the weight percentage of F decreased from the original 10–23% to 0–5%. Using X-ray photoelectron spectroscopy (XPS), the $Li_xPO_yF_z$ peak at 686.9 eV in F 1s spectra demonstrated an inverse relationship with Si content,[32] where the $Li_xPO_yF_z$ peak decreases as the Si content increases (Fig. S3c†). For the most stable graphite anodes, the peak of $Li_xPO_yF_z$ still existed after 72 h of storage. In contrast, all the Si-containing anodes showed no $Li_xPO_yF_z$ left (Fig. 1d).

Limited by characterization technology, the real-time kinetic process during calendar aging is still dimmish, including the Li^+ diffusion, transfer, and corresponding side reactions. Related simulations are thus introduced to demystify the mystery. The simulation results of cells with the graphite anode and the 10Si anode showed good consistency with the experimental data during the 0.1 C formation process (Fig. 1e). When leaving the fully charged full cells open circuit at RT for 24 h, the discharge data also demonstrated the same curve shape and capacity retention (Fig. 1f). Thus, the models established here are validated to reveal the self-discharge mechanism of cells with Si/C composite anodes.

Detailed aging process in the 10Si anode

When cells were rest after fully charged, the voltage dropped immediately due to polarization (Fig. 2a). For cells with 10Si anodes, the low conductivity of Si leads to a greater voltage drop to 4.154 V (*vs.* 4.166 V for graphite-based cells). The OCPs

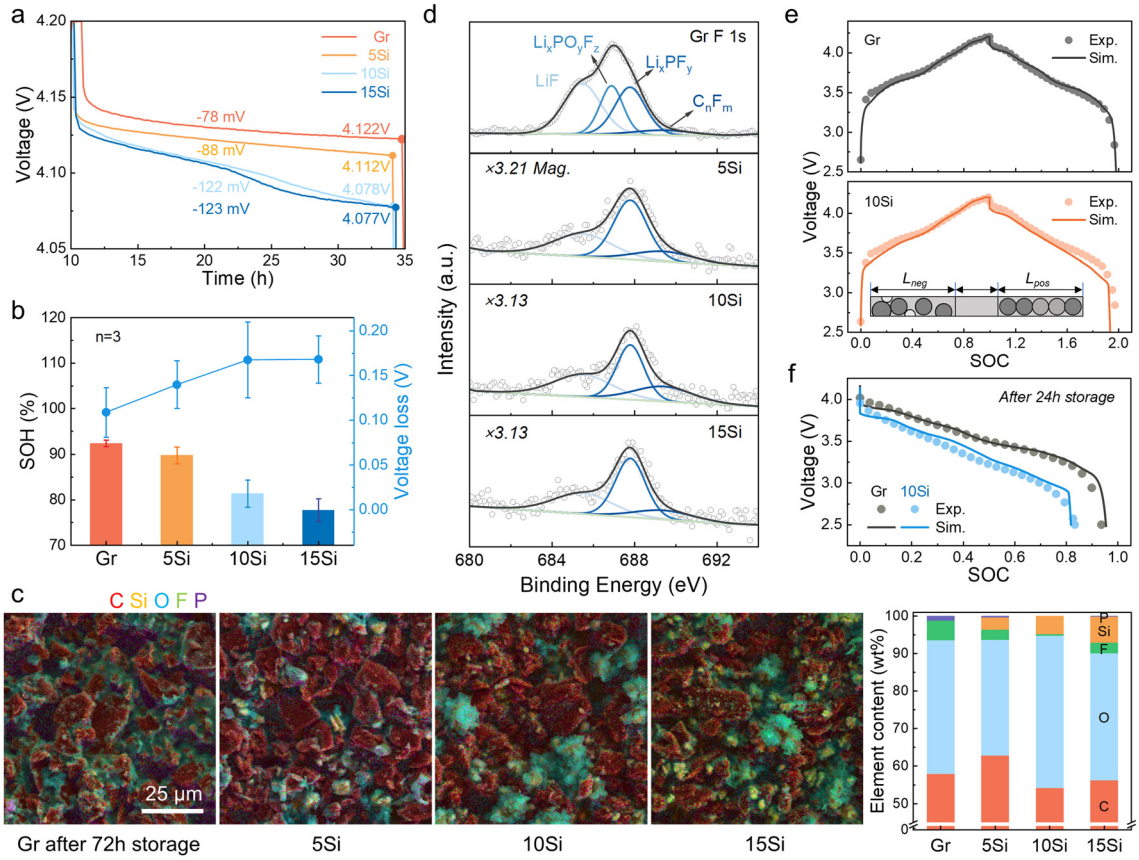

Fig. 1 Anode degradation validation and simulation introduction. (a) Voltage–time profiles of OCP drop for cells after charging to 4.2 V at 0.1 C. (b) SOH and voltage loss for cells after 24 h of storage. The error bar is calculated from 3 sets of cells. (c) SEM-EDS images and element content of anodes after 72 h of storage: the graphite, 5Si, 10Si, and 15 Si anode, respectively. (d) The F 1s spectra of the anodes suffering 72 h calendar aging. For the 5Si, 10Si, and 15Si anodes, the vertical axis range was amplified by 3.21, 3.13, and 3.13 times, respectively. (e and f) Model verification: (e) the voltage profiles of full cells with graphite anode and 10Si anode. (f) The discharging profiles of full cells after 24 h of storage.

of cathodes remained nearly constant and the voltage losses of full cells were mainly determined by the anodes, which was in agreement with the experimental data (Fig. S1†). The states of charge (SOC) of electrodes were calculated by dividing the remaining Li inventory in electrodes by the charging capacity (Fig. 2b).[33] The Li loss of the 10Si anode was much faster than that of the graphite anode, causing a nearly 3-fold increase in attenuation (8.7% *vs.* 2.3% in 24 h). Over the entire 24 h storage period, cells with 10Si anodes experienced a 17.6% capacity loss, while cells with graphite anodes showed only a 4.3% capacity reduction (Fig. 2c).

Through experiments and simulations, the Si/C composite anodes are proven to induce more severe Li loss than graphite anodes. But what interests us is the pathway of self-discharge caused by the unstable Si. As shown in Fig. 2d, when cells are placed in an open-circuit state, the calendar aging for graphite anode is influenced by only one active material. When taking account of the effect of Si, however, the aging mechanism becomes complicated. Specifically, are the decay rates for Si and graphite particles independent of each other, and would the side reaction of graphite be accelerated by Si? The simulation established here allows us to monitor these changes. In Fig. 2e, the SOC of particles refers to the average Li^+ concentration over the maximum Li^+ concentration of the material (c_{Li^+}/c_{max}).[34,35] For 10Si anodes, the SOC of graphite dropped rapidly from 0.874 to 0.739, while the SOC of Si decreased slowly from 0.842 to 0.771. The potential of Si increased rapidly with an increase of 18.8 mV during 24 h of storage, and the potential jump of graphite particles was faster than the one in graphite anode (3.7 mV *vs.* 2.1 mV, Fig. 2f).

A 2D model was introduced to unveil the kinetic process among AMs, *i.e.* Li^+ crosstalk (Fig. 3a and S4†).[36] The lithiation state along thickness was inhomogeneous even at 0.1 C charging. Graphite particles near the separator showed 0.909 SOC while only 0.906 was acquired near the Cu current collector (Fig. 3b and S5†). Once the charging process stopped, the Li^+ transferred from graphite to Si with a current density (I) around 100 mA m^{-2} (Fig. 3c–e). During the storage time, Si displayed a higher potential than graphite, thus a micro-loop was formed between Si and graphite, in which lithiated graphite was treated as a Li source. Driven by the overpotential, the Li^+ ions in graphite particles were forced to supply to Si (Fig. S6†). The mass and charge transport in the electrolyte are shown in Fig. 3f–m. I and c_{Li^+} changed more violently at charging than

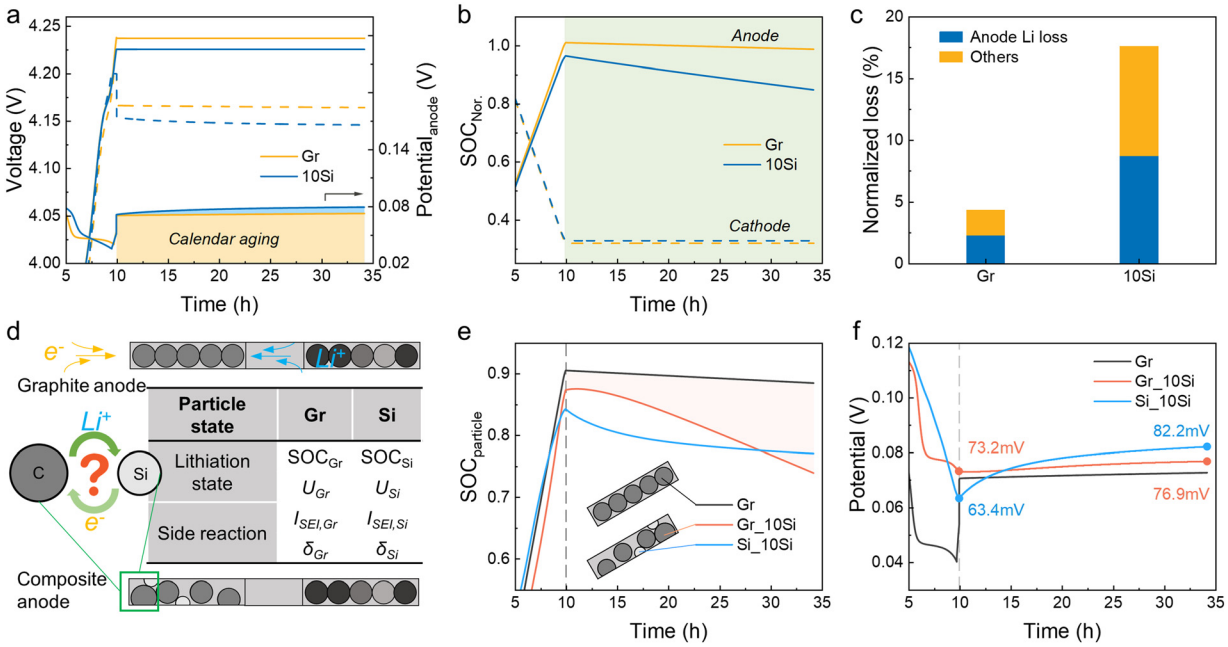

Fig. 2 The lithiation state comparisons between full cells with 10Si anode and cells with graphite anode during 24 h of storage by simulation. (a) The voltage profiles of full cell, cathode, and anode, respectively. (b) The SOC profiles of cathode and anode. (c) The normalized capacity loss with charging capacity as a benchmark. (d) The mechanism diagram illustrating changes in AMs effected by the Li^+ crosstalk. (e) The SOC profiles of graphite and Si particles in graphite anodes and 10 Si anodes. (f) The potential profiles of AMs.

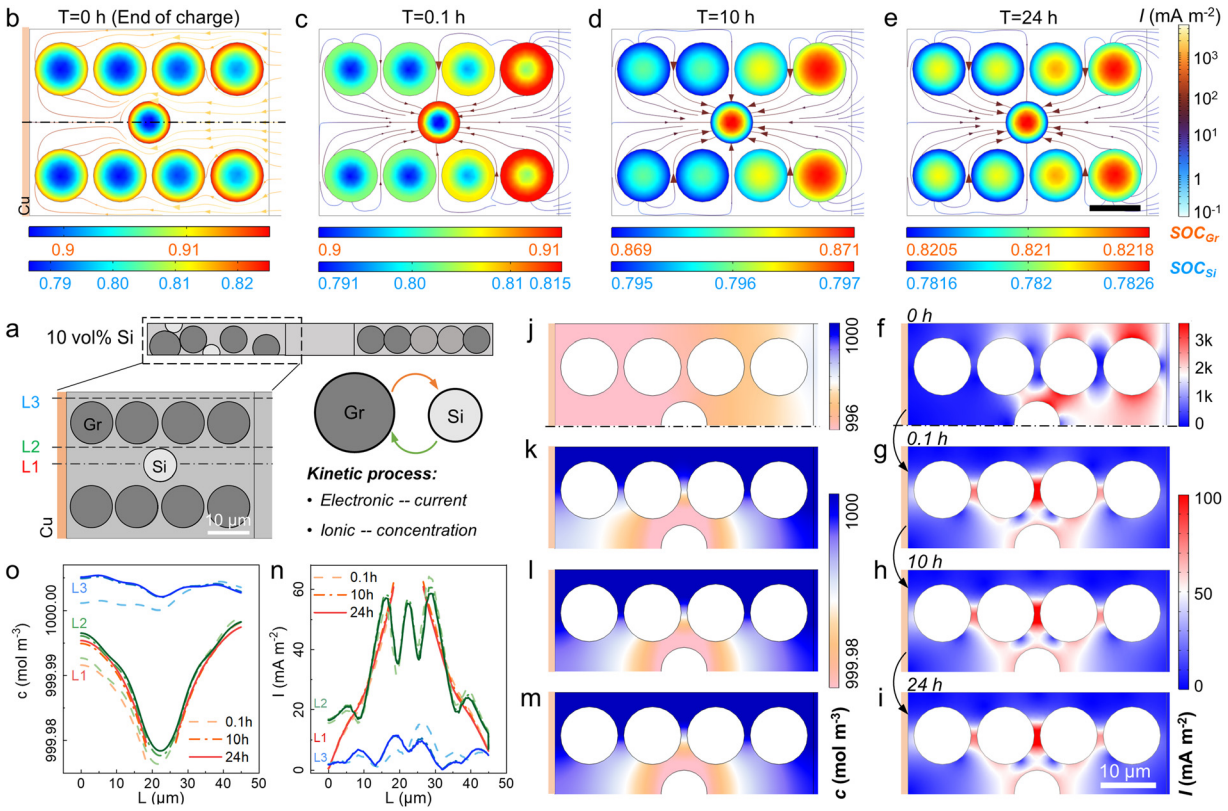

Fig. 3 The Li^+ crosstalk between graphite and Si particles during calendar aging. (a) The geometric structure of 10Si anode. (b–e) The c_{Li^+} distribution and Li^+ movement at different storage time: (b) 0 h (end of charge), (c) 0.1 h, (d) 10 h, and (e) 24 h. (f–i) The current field and (j–m) concentration field in the electrolyte at different storage time. (n and o) The line distribution of (n) I and (o) c_{Li^+} in the electrolyte at 3 locations marked in the inset (a).

in storage. Initially, the areas near the separator showed a higher I (>3 A m^{-2}, Fig. 3f), while c_{Li^+} varied along the thickness direction from 996 to 999 mol m^{-3} due to the external electric field (Fig. 3j). Once the external current vanished (t > 0 h), the side reaction current was higher near Si with a more prominent Li^+ depletion. The gradient of c_{Li^+} in Si transitioned from "lower inside and higher outside" to "higher inside and lower outside" at ~1.6 h when internal Li^+ supply cannot meet surface consumption (Fig. S7†). I and c_{Li^+} at three different locations were monitored, *i.e.* areas near the Si (L1 and L2) and near the graphite (L3). L2 and L3 were affirmed with the largest I and Li^+ consumption (Fig. 3n and o). The 10 vol% Si addition led to a 3-fold I increase and extra c_{Li^+} decrease than graphite-based cells (Fig. S8†).

The SEI growth was explored additionally (Fig. 4). The side reaction of Si was always dominant during the calendar aging (−90 to −70 mA m^{-2}, Fig. 4a). The side reaction current density (I_{SEI}) and areal capacity (Q_{SEI}) of graphite in 10Si anodes were lower than those in graphite anodes because the SOC of graphite and the corresponding overpotential of side reaction (η_{SEI}) in 10Si anodes was lower than in graphite anodes (Fig. 2e and f). The calculated thickness of SEI (δ_{SEI}) of graphite raised from 53 nm to 149 nm in 10Si anodes, while increased from 45 nm to 148 nm for graphite anodes (Fig. 4b). The Si addition promotes the SEI growth of graphite with greater I_{SEI}, especially during the charging process (Fig. 4a). Once the external current disappears, the δ_{SEI} of graphite in Si-containing anodes increases slowly due to the lower η_{SEI}.

To affirm the simulation results, the fully charged cells were stored at RT for 72 h and then dissembled. From SEM images (Fig. 4c and d), Si appeared as smooth, rounded chunks with a brighter color due to its lower conductivity, while graphite shows a distinct layered structure with a darker color. The SEI on 10Si anodes was indeed more luxuriant than graphite anodes. XPS depth profiling was conducted to determine the δ_{SEI} grown on each AM (Fig. 4e–g). The δ_{SEI} of graphite was specified when the Li_xC peak intensity at 282.2 eV equaled the C–C peak at 284.8 eV (Fig. 4e and f).[37] Similarly, the δ_{SEI} of Si was specified when the Li_xSi peak intensity at 97.2 eV equaled the Li_xSiO_y peak at 101.1 eV (Fig. 4g).[38] As a

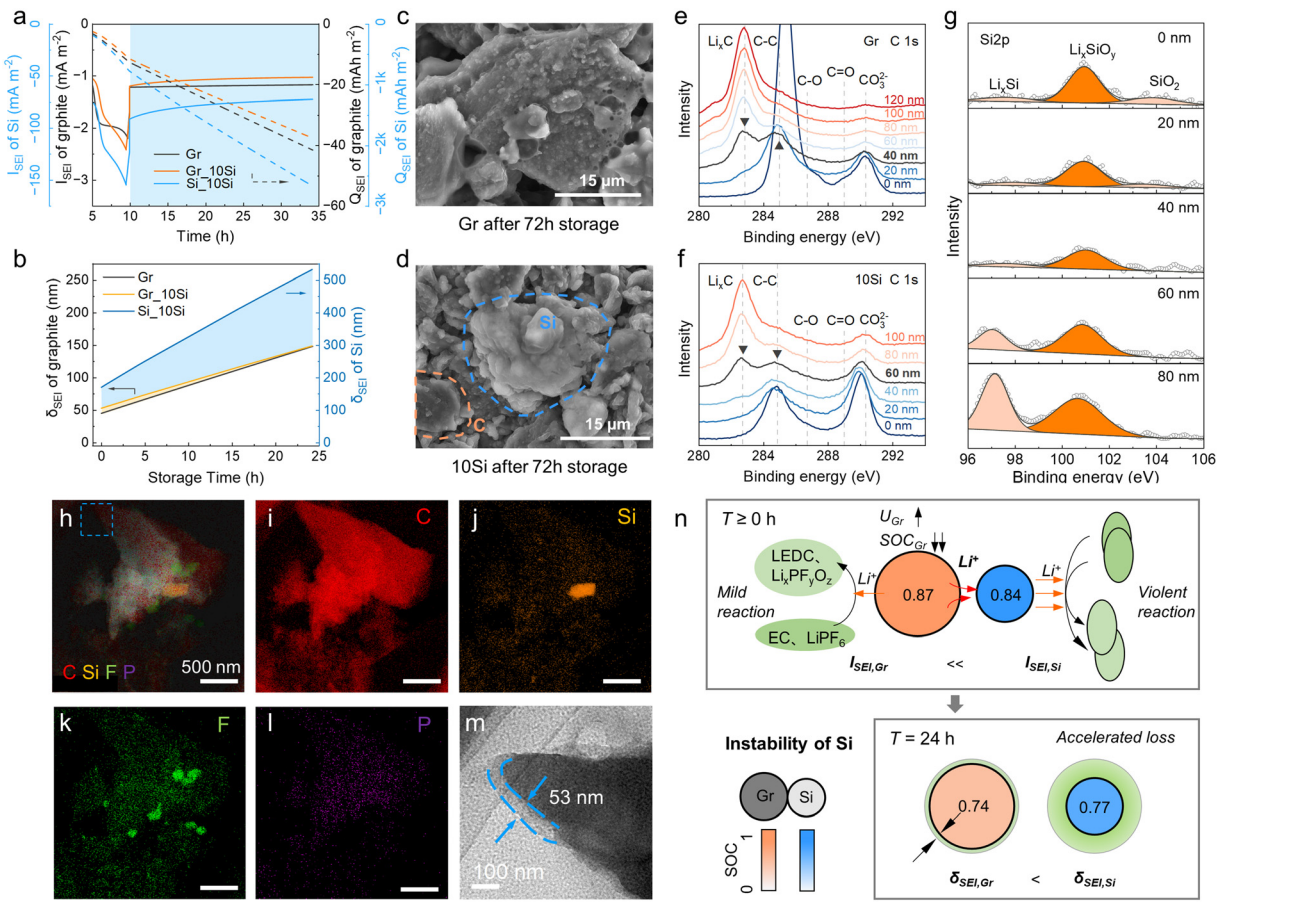

Fig. 4 The side reaction accelerated by active Si. (a) The calculated current density, I_{SEI}, and areal capacity, Q_{SEI} during storage. The I_{SEI} and Q_{SEI} of Si are plotted using blue lines. (b) The calculated δ_{SEI} profiles during storage. (c and d) SEM images of aged (c) graphite anode and (d) 10Si anode. (e and f) The C 1s XPS spectra depth profiles of aged (e) graphite anode and (f) 10Si anode (after 72 h of storage). (g) The Si 2p XPS spectra depth profiles of aged 10Si anode. (h–l) Elemental maps of aged 10Si anode and (m) the enlarged image in (h). (n) Schematic illustration of the kinetic process during calendar aging in Si-containing anodes.

result, the δ_{SEI} of graphite anodes was 40 nm, lower than 60 nm for the graphite in 10Si anodes. The δ_{SEI} of Si in 10Si anodes was 80 nm. An extra transmission electron microscopy (TEM) characterization reaffirmed the δ_{SEI} of graphite in 10Si anodes was thicker than that in graphite anodes (Fig. 4h–m).

Combining the experiments and simulations, the adverse impact of unstable Si on calendar life was clarified (Fig. 4n). Due to quite low conductivity and D_{Li^+} for Si, the lithiation state of Si-containing anodes is insufficient, thus the SOC of Si is lower than graphite. The active Si induces a quite severe side reaction during storage accompanied by prominent Li loss and potential rebound. Driven by the potential gradient, the Li^+ in graphite is forced to supply to Si, leading to an accelerated Li loss of graphite. As a result, the available capacity in Si-containing anodes plummets with a robust SEI growth.

The role of Si content in calendar aging

Increasing the Si content in anodes indeed enhances the energy density.[14] Regrettably, cells with high Si content anodes experience more severe self-discharge as mentioned above. To balance the relationship between energy density and service life, the effects of Si content were explored using the established model (Fig. 5). Cells with higher Si content were proved to suffer a larger voltage drop with less capacity retention (Fig. 5a and b). Before reaching a Si content of 40 vol%, the SOH decreased dramatically during the 24 h of storage period with increasing Si content (Fig. 5c). When the Si content exceeded 50%, the decay rate slowed down. The SOH of 24 h stored cells followed the relationship with Si content (x) as shown below:

$$\mathrm{SOH} = 21.09\mathrm{e}^{-x/10.35} + 74.48 \quad (1)$$

The potentials of anodes were monitored, showing an increase trend with a higher Si content (Fig. 5d). The remaining Li inventory in anodes decreased more rapidly with increasing Si content (Fig. 5e). By calculating the SOC decrease during 24 h of storage, the Li loss of the anode reached 2.3%, 11.6%, 14.7%, 16.5%, 17.3%, and 17.4%, respectively, when

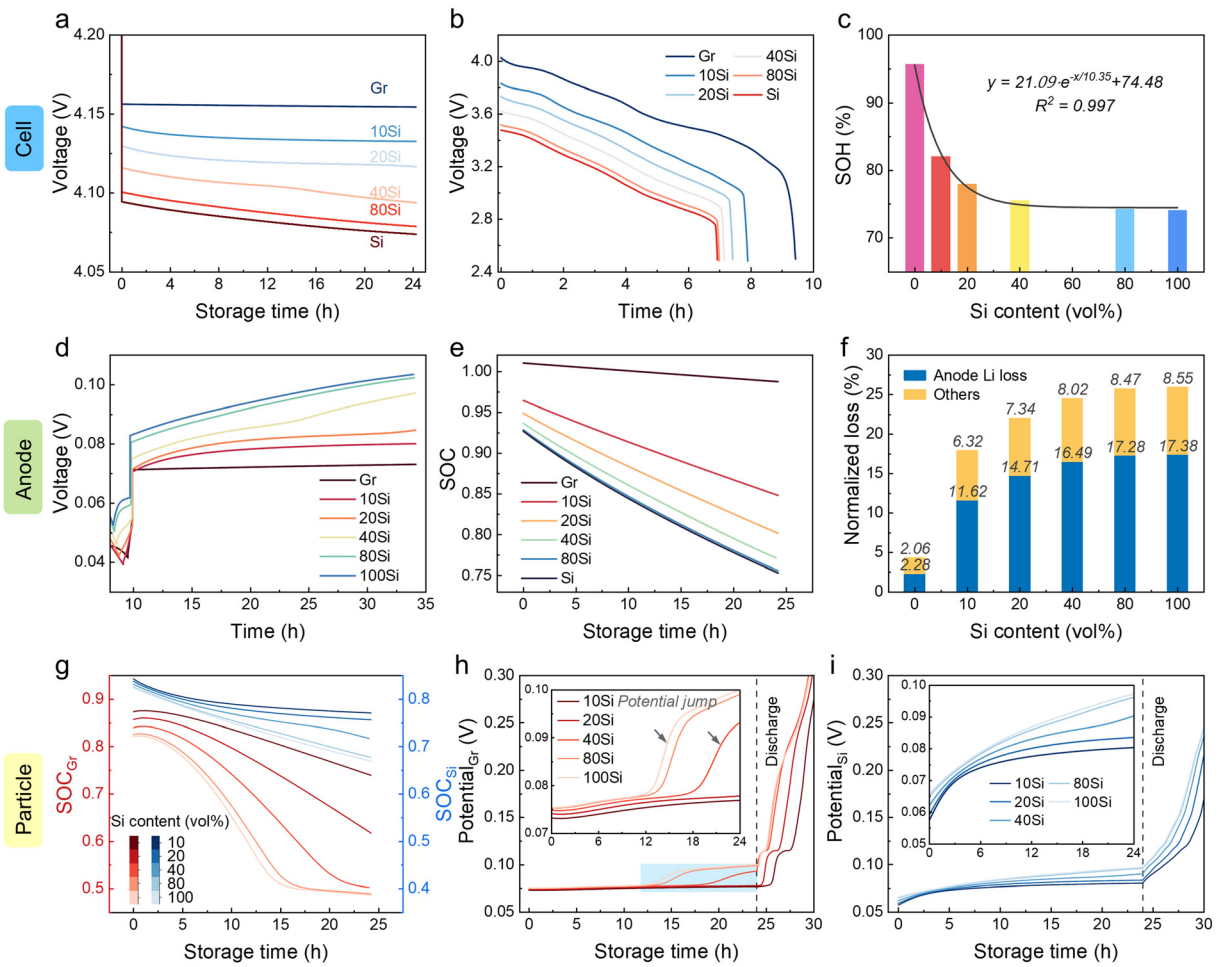

Fig. 5 The degradation effects brought by increasing Si content. (a–c) Decay prediction in cell level: (a) voltage profiles, (b) discharge profiles, and (c) SOH for full cells after 24 h of storage. (d–f) Decay prediction in electrode level: (d) potential rebound of anodes, (e) SOC profiles, and (f) normalized capacity loss bar charts. (g) The SOC profiles of graphite and Si particles. (h and i) The potential profiles of (h) graphite and (i) Si during storage. Insets in (h) and (i) are magnified views. "100Si" mentioned here refers to a Si content of 99.99 vol%.

the Si content was 0, 10%, 20%, 40%, 80%, and ~100% (Fig. 5f). The ratio of Li loss in the total capacity loss increased with the Si content. The Li inventory of graphite particles suffered from sharp attenuation compared with that of Si particles (Fig. 5g). For anodes with Si content of ~100%, the SOC of graphite decreased from 0.82 to 0.49, while shifted from 0.82 to 0.67 for Si. Considering the phase transfer stage at 0.07 V for graphite (LiC_6 to LiC_{12}), a huge Li loss leads to a potential jump, which was also shown in the experiment (Fig. 5h, i, and S1†). The time of this potential jump advanced from 19 h to 13 h as the Si content increased from 40% to ~100%.

For anodes with a higher Si content, the I_{SEI} and Q_{SEI} were detected with a decreasing trend (Fig. S9†). This is because η_{SEI} decreased due to insufficient capacity utilization (low SOC) when using an anode with a higher Si content. Accordingly, the SEI growth descended. Although the I_{SEI} and Q_{SEI} went down when the Si content increased, when it comes to the total capacity loss, the incremental reactive area of Si still caused a graver decay.

A self-discharge suppression method by adjusting Li^+ crosstalk

It is well-known that side reactions can be suppressed by AM coating,[39,40] while little attention is paid to the kinetic improvement. Since Si reacts severely and plunders Li^+ from graphite, enhancing the Li storage in Si by improving the D_{Li^+} may help suppress self-discharge. The D_{Li^+} of Si was set to 10-fold in the 10Si anode (marked as "$10D_{Li^+}$"), and the OCP of full cells was increased by 2 mV after 24 h of storage (Fig. 6a). After 24 h of storage, cells with improved 10Si anodes enabled a 7.7 h of 0.1 C discharging, showing a 5.5% increase in capacity retention than unimproved cells (7.3 h, Fig. 6b). When the anodes were fully charged (storage time at 0 h), the SOC of Si was improved from pristine 0.81 to 0.84 (Fig. 6c). Besides, the potential of Si in improved 10Si anodes was lower (65 mV *vs.* 74 mV) and rebounded with a greater speed (Fig. 6d). The Li loss from graphite was proven to be inhibited, showing a much lower SOC decrease of 0.067 and voltage rebound of 3.2 mV.

A larger D_{Li^+} of Si enabled more sufficient Li storage, which allowed Si to have a lower potential than graphite when fully charged (Fig. 6d). Once the current vanished, the Si served as Li sources and the Li^+ crosstalk was modified (Fig. S10 and S11† for details). Fig. 6e shows the Li^+ movement among AMs at the beginning of storage (T = 0.1 h). Different from the traditional 10Si anode (Fig. 3c), the Si provided Li^+ to the graphite, making up for the Li loss caused by the side reaction. The

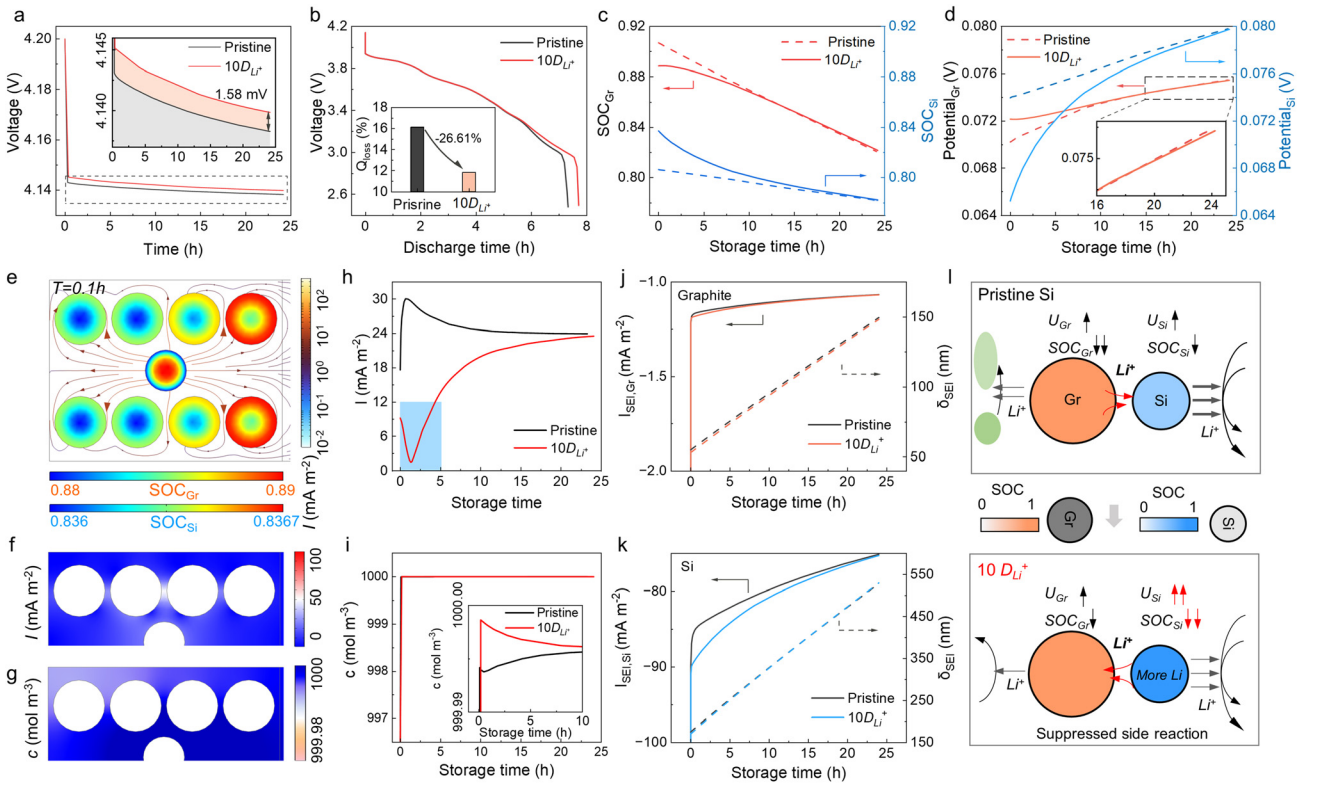

Fig. 6 Self-discharge suppression from the Li^+ crosstalk perspective by improving the D_{Li^+} of Si. (a) Voltage profiles between traditional full cells (marked as "Pristine") and the improved one (marked as "$10D_{Li^+}$"). (b) The discharge profiles and capacity loss (inset). (c) SOC profiles of graphite (left) and Si (right). (d) Potential profiles of graphite (left) and Si (right). (e) The c_{Li^+} distribution and ion movement, (f) current field, and (g) concentration field in improved Si after 0.1 h of storage. The profiles of (h) average I and (i) c_{Li^+} in the electrolyte during 24 h of storage. The inset in (i) is a magnified view. (j and k) The I_{SEI} and δ_{SEI} comparison of (j) graphite and (k) Si. (l) Schematic of improvement principle by controlling the Li^+ transfer direction.

distribution of I in the electrolyte was uniform and the value was less than 50 mA m^{-2} (Fig. 6f), much lower than the original condition (~100 mA m^{-2}). Besides, the distribution of c_{Li^+} was also more uniform, and less electrolyte was decomposed (Fig. 6g). When the storage time reached 1.4 h, the potential of Si rose close to the potential of graphite, and Li^+ no longer transferred from Si to graphite (Fig. S11†). After 1.4 h, Si no longer supplied Li^+ outwards, instead the graphite transferred Li^+ to Si (Fig. S10†). The Si with $10D_{Li^+}$ exhibits an effect similar to pre-lithiation in Si/C composite anodes, supplying extra Li.[41,42] During the storage, the gradient of c_{Li^+} in graphite was proven unchanged, and only the c_{Li^+} distribution in Si became more uniform (Fig. S12†).

Fig. 6h shows the I change with the storage time, and the improved 10Si anode exhibited a much lower I, especially in the first 5 h. In the traditional 10Si anode, I was 30.0 mA m^{-2} at 0.89 h; in contrast, 1.7 mA m^{-2} of I was shown in improved 10Si anodes. The Li^+ movement in anodes went milder and this improvement lasted for the whole storage time (Fig. S10b†). The consumption of electrolytes was somewhat inhibited as well (Fig. 6i and S10c†). As for the side reaction, the I_{SEI} of graphite and Si showed a little increase, and little changes were shown on the δ_{SEI} (Fig. 6j and k). Fig. 6l displays how the Si with improved D_{Li^+} suppresses the self-discharge during storage. The Si enabled extra Li storage, compensating for the Li loss of AMs and inhibiting the electrolyte consumption. The degree of suppression depends on the amount of Li stored in the Si, and once the additional Li is completely consumed, the calendar aging pathway will revert to the conventional mode.

Inhibited calendar aging by kinetic enhancement

To improve the D_{Li^+} of Si, nano-Si was deposited in porous carbon (marked as "Si@C") by chemical vapor deposition (CVD). As shown in Fig. 7a, the pristine Si exhibits an ordered crystal structure. The TEM image of Si@C demonstrates ordered (201) Si embedded in a disordered carbon matrix, while the selected area electron diffraction (SAED) exhibits characteristics of long-range disorder (Fig. 7b). The elemental mapping shows that Si and C are uniformly distributed throughout the Si@C particles (Fig. 7c).

The previous analysis demonstrated that higher Si content leads to more pronounced self-discharge. To test the improvement brought by this material, anodes with 15 wt% Si were

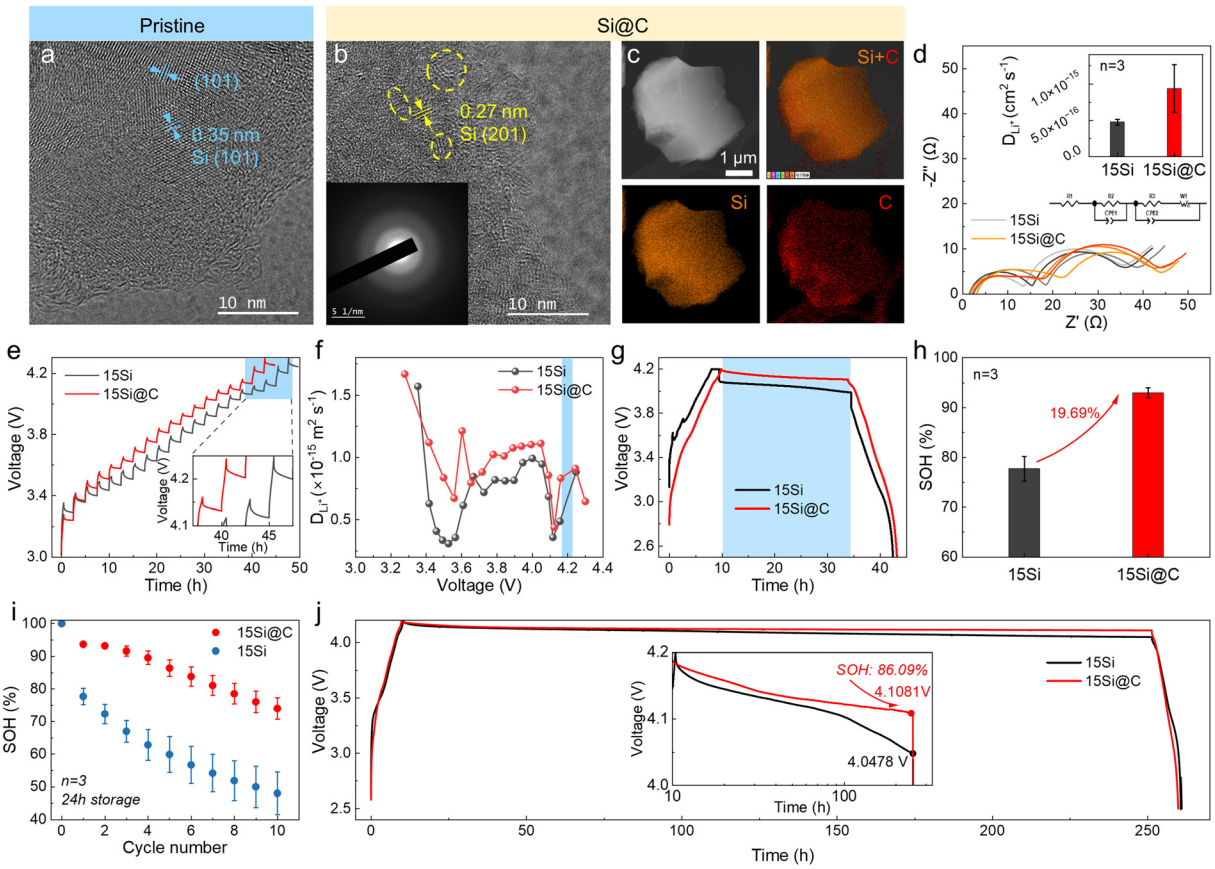

Fig. 7 Improved calendar life by increasing the D_{Li^+} of Si. (a and b) TEM image of (a) pristine Si and (b) Si@C. (c) Elemental maps of Si@C particle. (d) EIS profiles of full cells at 4.2 V and calculated D_{Li^+} (inset). (e) GITT test of full cells with 15Si and 15Si@C anodes. The inset is a magnified view. (f) The D_{Li^+} in cells during charging. (g) Voltage profiles with 24 h of storage. (h) The SOH comparison after 24 h of storage. (i) The SOH changes for 24 h of storage with 10 times repeating. (j) Voltage profiles under more than 240 h of storage. The inset shows the voltage change when the timeline is logarithmic.

fabricated (Fig. S13†). The electrochemical impedance spectroscopy (EIS) result of the fully charged battery showed a typical shape of 2 circles in the high- and middle-frequency ranges plus 1 line in the low-frequency range (Fig. 7d).[43] The ohmic resistance (R_Ω), SEI resistance (R_{SEI}), and charge transfer resistance (R_{ct}) were calculated using the equivalent circuit presented in Fig. 7d. The interfacial impedance was shown a little larger for cells with 15Si@C anodes (Table S2†), but the D_{Li^+} at 4.2 V was calculated to be 2-fold higher than 15Si anodes (Note S1†).[44] Fig. 7e demonstrates the potential profiles using galvanostatic intermittent titration technique (GITT). The D_{Li^+} at 4.2 V was 9×10^{-16} m^2 s^{-1} for cells with 15Si@C anodes, and 7×10^{-16} m^2 s^{-1} for 15Si anodes, reaffirming a higher D_{Li^+} for 15Si@C anodes (Fig. 7f, S14, and Note S2†).[45,46] The OCP of full cells with 15Si@C anodes was indeed larger than that for 15Si anodes during storage (Fig. 7g). After 24 h of storage, the SOH of cells with 15Si@C anodes was 93.0%, showing a 20% increase to cells with 15Si anodes (77.7%), as shown in Fig. 7h. Besides, a 10 times 24 h storage test was repeated, and the cells with 15Si@C anodes displayed much more stable capacity retention. After 10 times repeating, the SOH of cells with 15Si@C anodes maintained at 74.0%, while the traditional cells decayed to 48.1% (Fig. 7i). The advantages of the pre-lithiation effect still remained after 240 h of storage (with SOH of 86.1%) but were depleted after 300 h of storage (Fig. 7j and S15†).

Conclusions

In summary, a real-time kinetic process during calendar aging was revealed for cells with Si/C composite anodes. The unstable Si induced severe side reactions, causing a massive Li loss. Driven by the potential difference, the graphite was forced to supply Li^+ to Si. As a result, graphite was affected by Si to perform more unstably during storage, with a fast Li loss and a thicker SEI film growth of 60 nm (*vs.* 40 nm for graphite anode) after 72 h of storage. Besides, the ion transfer and electrolyte consumption were aggravated by the Si addition. For cells with 10Si anodes, the max current density of self-discharge was 30.0 mA m^{-2}, 3 times larger than that for graphite anodes, and the electrolyte concentration was decreased below 1000 mol m^{-3}. An innovative method to suppress self-discharge was proposed by adjusting the aging pathway, *i.e.* converting the Li^+ crosstalk between graphite and Si. The self-discharge was found to be inhibited by increasing the D_{Li^+} of Si, which enabled a more sufficient Li storage to change the movement from "graphite to Si" to "Si to graphite". The ion transfer in electrolyte was inhibited to 1.7 mA m^{-2}, and the electrolyte concentration can maintain ~1000 mol m^{-3}. As a proof of concept, full cells with two kinds of Si-containing anodes were fabricated: the traditional Si and Si@C with nano-Si embedded in a carbon matrix. A 15 wt% of Si content was added in anodes, and the D_{Li^+} was improved from 7×10^{-16} m^2 s^{-1} to 9×10^{-16} m^2 s^{-1} once cells were fully charged. After 24 h of storage, the SOH was increased from 74.1% to 93.1%. This work enhances the understanding of calendar aging mechanisms in Si/C composite anodes, aiding the development of cells with extended service life.

Author contributions

Kai Sun: conceptualization, methodology, investigation, writing – original draft preparation; Xueyan Li: investigation, methodology; Kang Fu: investigation; Zhuojun Zhang: visualization; Anmin Wang: methodology; Xingmin He: investigation; Lili Gong: conceptualization, investigation; methodology; Peng Tan: conceptualization, writing – review & editing, supervision, project administration, funding acquisition.

Data availability

All relevant data are included in this article and the ESI.†

Conflicts of interest

There are no conflicts to declare.

Acknowledgements

We acknowledge the funding support from National Key R&D Program of China (2023YFB2408100), and Anhui Provincial Natural Science Foundation of China (2308085QG231). This work was partially carried out at the Instruments Center for Physical Science, University of Science and Technology of China.

References

1 C.-Y. Wang, T. Liu, X.-G. Yang, S. Ge, N. V. Stanley, E. S. Rountree, Y. Leng and B. D. McCarthy, *Nature*, 2022, **611**, 485–490.
2 CATL, 2022, **https://www.catl.com/news/6467.html**.
3 J. Xie and Y.-C. Lu, *Nat. Commun.*, 2020, **11**, 2499.
4 C. P. Grey and D. S. Hall, *Nat. Commun.*, 2020, **11**, 6279.
5 H. L. Andersen, L. Djuandhi, U. Mittal and N. Sharma, *Adv. Energy Mater.*, 2021, **11**, 2102693.
6 Y. Gao, Z. Pan, J. Sun, Z. Liu and J. Wang, *Nano-Micro Lett.*, 2022, **14**, 94.
7 K. Sun, X. Xiao, W. Shang, K. Fu, X. Li, Z. Zhang, L. Gong and P. Tan, *Small*, 2024, 2405674.
8 X. Su, Q. Wu, J. Li, X. Xiao, A. Lott, W. Lu, B. W. Sheldon and J. Wu, *Adv. Energy Mater.*, 2014, **4**, 1300882.
9 W. Dou, M. Zheng, W. Zhang, T. Liu, F. Wang, G. Wan, Y. Liu and X. Tao, *Adv. Funct. Mater.*, 2023, **33**, 2305161.
10 M. Bai, X. Tang, M. Zhang, H. Wang, Z. Wang, A. Shao and Y. Ma, *Nat. Commun.*, 2024, **15**, 1–13.

11 M. T. McDowell, S. W. Lee, J. T. Harris, B. A. Korgel, C. Wang, W. D. Nix and Y. Cui, *Nano Lett.*, 2013, **13**, 758–764.
12 S. W. Lee, M. T. McDowell, J. W. Choi and Y. Cui, *Nano Lett.*, 2011, **11**, 3034–3039.
13 F. Luo, B. Liu, J. Zheng, G. Chu, K. Zhong, H. Li, X. Huang and L. Chen, *J. Electrochem. Soc.*, 2015, **162**, A2509–A2528.
14 S. Chae, S. Choi, N. Kim, J. Sung and J. Cho, *Angew. Chem., Int. Ed.*, 2020, **59**, 110–135.
15 L. Sun, Y. Liu, L. Wang and Z. Jin, *Adv. Funct. Mater.*, 2024, **34**, 2403032.
16 J. Sung, N. Kim, J. Ma, J. H. Lee, S. H. Joo, T. Lee, S. Chae, M. Yoon, Y. Lee, J. Hwang, S. K. Kwak and J. Cho, *Nat. Energy*, 2021, **6**, 1164–1175.
17 X. Zhang, D. Wang, X. Qiu, Y. Ma, D. Kong, K. Müllen, X. Li and L. Zhi, *Nat. Commun.*, 2020, **11**, 3826.
18 K. Ge, Z. Wang, J. Liu, Y. Mu, R. Wang, X. Xu, Y. Wang, Z. Zou, Q. Zhang, M. Han and L. Zeng, *Adv. Funct. Mater.*, 2024, 2414384.
19 C. Sun, H. Zhang, P. Mu, G. Wang, C. Luo, X. Zhang, C. Gao, X. Zhou and G. Cui, *ACS Nano*, 2024, **18**, 2475–2484.
20 H. Cheng, Z. Ma, P. Kumar, H. Liang, Z. Cao, H. Xie, L. Cavallo, H. Kim, Q. Li, Y. Sun and J. Ming, *Adv. Energy Mater.*, 2024, **14**, 2304321.
21 H. Jia, X. Li, J. Song, X. Zhang, L. Luo, Y. He, B. Li, Y. Cai, S. Hu, X. Xiao, C. Wang, K. M. Rosso, R. Yi, R. Patel and J.-G. Zhang, *Nat. Commun.*, 2020, **11**, 1474.
22 J. D. McBrayer, M.-T. F. Rodrigues, M. C. Schulze, D. P. Abraham, C. A. Apblett, I. Bloom, G. M. Carroll, A. M. Colclasure, C. Fang, K. L. Harrison, G. Liu, S. D. Minteer, N. R. Neale, G. M. Veith, C. S. Johnson, J. T. Vaughey, A. K. Burrell and B. Cunningham, *Nat. Energy*, 2021, **6**, 866–872.
23 N. Kim, Y. Kim, J. Sung and J. Cho, *Nat. Energy*, 2023, **8**, 921–933.
24 I. Zilberman, J. Sturm and A. Jossen, *J. Power Sources*, 2019, **425**, 217–226.
25 K. Bischof, M. Flügel, M. Hölzle, M. Wohlfahrt-Mehrens and T. Waldmann, *J. Electrochem. Soc.*, 2024, **171**, 010510.
26 W. Lu, L. Zhang, Y. Qin and A. Jansen, *J. Electrochem. Soc.*, 2018, **165**, A2179–A2183.
27 K. Kalaga, M.-T. F. Rodrigues, S. E. Trask, I. A. Shkrob and D. P. Abraham, *Electrochim. Acta*, 2018, **280**, 221–228.
28 Y. Yin, E. Arca, L. Wang, G. Yang, M. Schnabel, L. Cao, C. Xiao, H. Zhou, P. Liu, J. Nanda, G. Teeter, B. Eichhorn, K. Xu, A. Burrell and C. Ban, *ACS Appl. Mater. Interfaces*, 2020, **12**, 26593–26600.
29 T. Gao, Y. Han, D. Fraggedakis, S. Das, T. Zhou, C.-N. Yeh, S. Xu, W. C. Chueh, J. Li and M. Z. Bazant, *Joule*, 2021, **5**, 393–414.
30 X. Lu, M. Lagnoni, A. Bertei, S. Das, R. E. Owen, Q. Li, K. O'Regan, A. Wade, D. P. Finegan, E. Kendrick, M. Z. Bazant, D. J. L. Brett and P. R. Shearing, *Nat. Commun.*, 2023, **14**, 5127.
31 K. Sun, Z. Zhang, F. Kang, L. Xueyan, X. Xu, Y. Jianwen, G. Lili and T. Peng, *Nano Lett.*, 2025, DOI: **10.1021/acs.nanolett.4c03530**.
32 J. Huang, H. Zhang, X. Yuan, Y. Sha, J. Li, T. Dong, Y. Song and S. Zhang, *Chem. Eng. J.*, 2023, **464**, 142578.
33 K. Fu, X. Li, K. Sun, Z. Zhang, H. Yang, L. Gong, G. Qin, D. Hu, T. Li and P. Tan, *Adv. Funct. Mater.*, 2024, 2409623.
34 X. Gao, S. Li, J. Xue, D. Hu and J. Xu, *Adv. Energy Mater.*, 2023, **13**, 2202584.
35 X. Duan, D. Hu, W. Chen, J. Li, L. Wang, S. Sun and J. Xu, *Adv. Energy Mater.*, 2024, **14**, 2400710.
36 J. Moon, H. C. Lee, H. Jung, S. Wakita, S. Cho, J. Yoon, J. Lee, A. Ueda, B. Choi, S. Lee, K. Ito, Y. Kubo, A. C. Lim, J. G. Seo, J. Yoo, S. Lee, Y. Ham, W. Baek, Y.-G. Ryu and I. T. Han, *Nat. Commun.*, 2021, **12**, 2714.
37 K. Sun, X. Li, Z. Zhang, K. Fu, X. Xiao, L. Gong and P. Tan, *Energy Storage Mater.*, 2024, **66**, 103216.
38 W. Huang, J. Li, K. Wei and L. Wang, *J. Alloys Compd.*, 2024, **990**, 174416.
39 L. C. Merrill, D. M. Long, K. A. Small, K. L. Jungjohann, K. Leung, K. L. Bassett and K. L. Harrison, *J. Phys. Chem. C*, 2022, **126**, 17490–17501.
40 Z. Chen, Y. Qin, K. Amine and Y.-K. Sun, *J. Mater. Chem.*, 2010, **20**, 7606.
41 C. Yang, H. Ma, R. Yuan, K. Wang, K. Liu, Y. Long, F. Xu, L. Li, H. Zhang, Y. Zhang, X. Li and H. Wu, *Nat. Energy*, 2023, **8**, 703–713.
42 S.-Y. Ham, E. Sebti, A. Cronk, T. Pennebaker, G. Deysher, Y.-T. Chen, J. A. S. Oh, J. B. Lee, M. S. Song, P. Ridley, D. H. S. Tan, R. J. Clément, J. Jang and Y. S. Meng, *Nat. Commun.*, 2024, **15**, 2991.
43 S. Wang, J. Zhang, O. Gharbi, V. Vivier, M. Gao and M. E. Orazem, *Nat. Rev. Methods Primmers*, 2021, **1**, 41.
44 E. Hüger, D. Uxa and H. Schmidt, *J. Phys. Chem. C*, 2024, **128**, 7408–7423.
45 A. Nickol, T. Schied, C. Heubner, M. Schneider, A. Michaelis, M. Bobeth and G. Cuniberti, *J. Electrochem. Soc.*, 2020, **167**, 090546.
46 T. Schied, A. Nickol, C. Heubner, M. Schneider, A. Michaelis, M. Bobeth and G. Cuniberti, *ChemPhysChem*, 2021, **22**, 885–893.